

Effects of relaxation and interchannel coupling in inner-shell photoionization of atomic ytterbium

M. Kutzner

Physics Department, Andrews University, Berrien Springs, Michigan 49104

V. Radojević

Institute of Physics, P.O. Box 57, 11000 Belgrade, Yugoslavia

(Received 8 October 1993)

Photoionization cross sections, branching ratios, and photoelectron angular-distribution asymmetry parameters have been calculated for the Yb ($Z=70$) $4f$, $4d$, and $6s$ subshells using the relativistic random-phase approximation, the truncated relativistic random-phase approximation, and the relativistic random-phase approximation, modified to include relaxation effects. Comparisons are made between the various approximations and experimental data. Important relaxation effects for the $4f$ and $4d$ channels are noted and strong effects of interchannel coupling are noted for $6s$ photoionization in the region near the $4f$ and $5p$ thresholds.

PACS number(s): 32.80.Hd, 32.80.Fb

I. INTRODUCTION

The photoionization of inner shells of atoms is an important tool for probing interesting many-body effects. The relaxation of the ion having the inner-shell hole can lead to photoionization with excitation, double photoionization, and for some systems a radical redistribution of oscillator strength near threshold [1,2]. Previous studies have shown that the effects of core relaxation are especially important in the so-called "giant-resonance" regions of the spectrum found above the thresholds of channels having significant centripetal barriers [1,2].

Both the random-phase approximation with exchange (RPAE) [2] and its relativistic generalization, the relativistic random-phase approximation (RRPA) [3], have been found to give excellent agreement with experiment for many closed-shell systems because they effectively include intrachannel and interchannel coupling among single-excitation channels to all orders in perturbation theory. The generalized RPAE (GRPAAE) [2] and the relativistic random-phase approximations modified to include relaxation (RRPAR) [4] were developed to incorporate effects of core relaxation into the theory. Recent papers reported the effects of relaxation in alkaline-earth-metal atoms [5] and group-IIIB atoms [6]. Photoionization cross sections from nd subshells (especially the $4d$ subshells) were shown to be significantly influenced by the relaxation effects, while for mercury the $4f$ cross section was brought into good agreement with experiment when relaxation was included using the RRPAR method.

Ytterbium ($Z=70$) with configuration $[\text{Xe}]4f^{14}6s^2$ is another example of a closed-shell atom with a $4f$ inner subshell that has been studied both experimentally [7] and theoretically [7]. Svensson *et al.* [7] reported ESSR (electron spectrometry using synchrotron radiation) measurements of Yb cross sections, branching ratios, and photoelectron angular-distribution asymmetry parameters over the range of photon energies from 17.5 to 100 eV. However, in the absence of an absolute measurement of the total photoabsorption cross section for ytterbium vapor, the normalization of the experimental data is arbi-

trary. Truncated RRPA calculations coupling a limited number of photoionization channels were found to be in reasonable agreement with experiment so far as cross section was concerned when the experiment was normalized to the theory at one energy point. There were, however, important differences between the experimental measurements of the angular-distribution asymmetry parameter and the truncated RRPA results. More complete RRPA calculations [8] (including 21 relativistic dipole channels) were soon reported above 40 eV, demonstrating the importance of interchannel coupling between channels from the $4f$ subshell and those from the $5p$ subshell.

In this paper, we report on the effects of core relaxation on the photoionization of $4f$ and $4d$ electrons of Yb. The importance of interchannel coupling on the $4f$ cross section is demonstrated below the $5p$ photoionization thresholds. No experimental data have yet been reported for the $4d$ photoionization of Yb. However, the construction of new synchrotron light sources may stimulate further studies of Yb and other systems at higher photon energies. Also, RRPA $6s$ photoionization parameters are reported and compared with the experiment [7].

In Sec. II, we briefly review the theory and methods of the RRPAR. Results are reported for the $4f$, $4d$, and $6s$ subshells in Sec. III and in Sec. IV some of the implications of the study are discussed.

II. METHOD

Detailed discussions of both the RRPA and the RRPAR can be found elsewhere [3,4]. Here I will point out that in the RRPA, the partial photoionization cross section for a given subshell is given by

$$\sigma_{n\kappa} = \frac{4\pi^2\alpha\omega}{3} (|D_{nj \rightarrow j-1}|^2 + |D_{nj \rightarrow j}|^2 + |D_{nj \rightarrow j+1}|^2). \quad (1)$$

Here n is the principal quantum number, $\kappa = \mp(j+1/2)$ for $j = l \pm 1/2$, where j and l are the single-electron total and orbital angular-momentum quantum numbers. The dipole matrix element $D_{nj \rightarrow j'}$ is the reduced RRPA dipole matrix element for the photoionization channel $nj \rightarrow j'$.

The angular-distribution asymmetry parameter $\beta_{n\kappa}$ for the subshell $n\kappa$ is defined in terms of the differential cross section as

$$\frac{d\sigma_{n\kappa}}{d\Omega} = \frac{\sigma_{n\kappa}(\omega)}{4\pi} [1 - \frac{1}{2}\beta_{n\kappa}(\omega)P_2(\cos\theta)], \quad (2)$$

where ω is the photon energy and θ is the angle measured between the directions of the incident photon and the photoelectron. When a subshell is split by spin-orbit splitting into two different levels $j = l \pm 1/2$, it is conventional to use the weighted average given by

$$\beta_{nl} = \frac{\sum_{\substack{\kappa = -(l+1), l \\ \kappa \neq 0}} \beta_{n\kappa} \sigma_{n\kappa}}{\sum_{\substack{\kappa = -(l+1), l \\ \kappa \neq 0}} \sigma_{n\kappa}}. \quad (3)$$

The RRPAP method approximates the effects of core relaxation by calculating the continuum photoelectron orbitals in the potential of the relaxed ion. The ionic core with the hole in the level with $j = l + 1/2$ has a lower ionization threshold energy and also represents the most populated of the two levels. Thus we generally place the hole in the subshell with largest j for the purpose of obtaining V^{N-1} potential. Overlap integrals of the form $\prod_i \langle \phi'_i | \phi_i \rangle^{q_i}$ between orbitals of the unrelaxed ground state ϕ_i and the corresponding orbitals of the final relaxed state ϕ'_i are included in the RRPAP dipole matrix element for each subshell i of the ion with occupation number q_i . Inclusion of these overlap integrals is important for calculations of partial photoionization cross sections since they approximately remove oscillator strength due to double-excitation processes from the single-excitation channel oscillator strength [9]. It should be noted that overlap integrals between orbitals of the ground state and the continuum orbitals of the final state have not been included. Thus oscillator strength due to Auger processes has not been removed from the main-line partial cross sections.

Photoionization thresholds in the strict RRPA model are the Dirac-Hartree-Fock (DHF) eigenvalues. However, experimental thresholds are frequently utilized. Here, we have used DHF threshold energies for RRPA calculations. In the RRPAP, I have used the experimental ionization energies [10] for calculations involving relaxation of a $4f$ hole. In the case of photoionization of $4d$ electrons, experimental ionization energies are not available and so the difference in the total relativistic self-consistent energies of the neutral atom and the ion (so-called ΔE_{SCF}) were used. The DHF and ΔE_{SCF} energies used here were obtained using the Oxford multiconfiguration Dirac-Fock computer code of Grant *et al.* [11]. Table I contains DHF, ΔE_{SCF} , and experimental threshold energies obtained using photoelectron spectroscopy for all the channels incorporated in the present study.

The RRPA theory predicts results which are gauge independent provided that one has included all possible dipole-excited channels [3]. In practice, where one limits the number of channels (the truncated RRPA), there will be differences between the "length-" and "velocity-"

TABLE I. Photoionization thresholds in a.u. for subshells of atomic ytterbium included in the present calculations. The third column lists the absolute values of single-particle eigenvalues from Dirac-Hartree-Fock (DHF) calculations. The fourth column lists the differences of self-consistent DHF calculations for the ground states and ionic states. The experimental values are from Ref. [10].

| Shell | J | DHF | Threshold | |
|-------|---------------|--------|-------------------------|----------|
| | | | ΔE_{SCF} | Expt. |
| $4d$ | $\frac{3}{2}$ | 7.7776 | 7.334 | |
| $4d$ | $\frac{5}{2}$ | 7.4221 | 6.993 | |
| $5s$ | $\frac{1}{2}$ | 2.4400 | | |
| $5p$ | $\frac{3}{2}$ | 1.4189 | | |
| $5p$ | $\frac{1}{2}$ | 1.1827 | | |
| $4f$ | $\frac{5}{2}$ | 0.5389 | 0.2136 | 0.373 66 |
| $4f$ | $\frac{7}{2}$ | 0.4801 | 0.1658 | 0.3274 |
| $6s$ | $\frac{1}{2}$ | 0.1965 | | 0.2298 |

gauge results. Also, the inclusion of relaxation effects in the RRPAP potential leads to differences in calculations performed in the two gauges. In this paper, results of calculations performed in the RRPA with large numbers of channels ($n \geq 15$) included have only the length result shown in the figures; RRPAP and truncated RRPA results have both length and velocity results plotted individually.

III. RESULTS

A. The $4f$ subshell

In the $4f$ photoionization calculations, 15 jj -coupled channels obtained by dipole excitation of the appropriate subshells were considered:

$$5s_{1/2} \rightarrow \epsilon p_{1/2}, \epsilon p_{3/2},$$

$$5p_{1/2} \rightarrow \epsilon d_{3/2}, \epsilon s_{1/2},$$

$$5p_{3/2} \rightarrow \epsilon d_{3/2}, \epsilon d_{5/2}, \epsilon s_{1/2},$$

$$4f_{5/2} \rightarrow \epsilon g_{7/2}, \epsilon d_{3/2}, \epsilon d_{5/2},$$

$$4f_{7/2} \rightarrow \epsilon g_{7/2}, \epsilon g_{9/2}, \epsilon d_{7/2},$$

and

$$6s_{1/2} \rightarrow \epsilon p_{1/2}, \epsilon p_{3/2}.$$

Results of the RRPA and RRPAP calculations of the $4f$ partial cross section of Yb are shown in Fig. 1. For the RRPA calculations, the length and velocity cross sections agree almost perfectly and so only the length result is shown. Length and velocity calculations are shown separately for the RRPAP. The ESSR measurements [7] are also shown for comparison. It should be noted that the ESSR experiments have been scaled to the geometric mean of length and velocity of the RRPAP calculations at 1.47 a.u.; the original experimental results were scaled

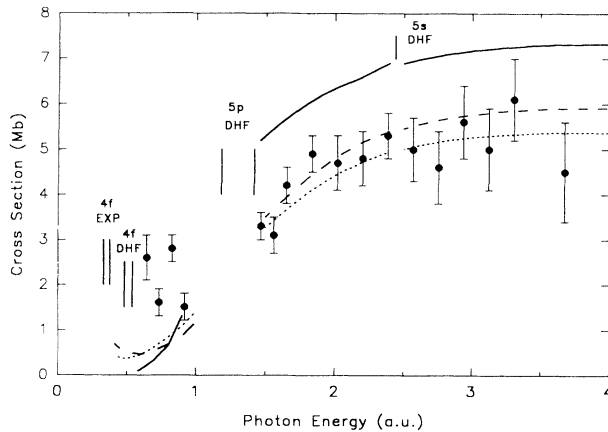


FIG. 1. Partial photoionization cross section for the $4f$ subshell of atomic Yb. Solid curve represents RRPA; long-dashed curve and short-dashed curve represent length and velocity RRPAR calculations, respectively. Experimental data, Ref. [7], are scaled to geometric mean of RRPAR length and velocity at 1.47 a.u. (40 eV).

to the truncated RRPA calculations at this energy [7]. Normalization to the RRPAR calculations is reasonable since the RRPAR approximately excludes the oscillator strength of satellite and double-photoionization channels from the $4f$ partial cross section. The calculations were not carried out below the $5p$ and $5s$ thresholds since autoionization resonances in these regions greatly complicate the calculations. Calculations combining the RRPA and the multichannel quantum-defect theory (MQDT) have been carried out in the resonance regions [7]. The experimental $4f$ thresholds used in the RRPAR calculations and the Dirac-Hartree-Fock thresholds used in the RRPA calculations are demarcated in the figure.

As in the case of mercury $4f$ photoionization [6], the effect of a large centripetal barrier in the potential for continuum eg orbitals causes the cross section to rise slowly from threshold to a fairly flat level which is maintained out to very high photon energies (at 10 a.u. the RRPA $4f$ partial cross section is still approximately 5.2 Mb). The inclusion of relaxation effects in the calculation has the effect of reducing the slope of the cross section near threshold. Evidently, oscillator strength is being redistributed to higher energies. By 4 a.u., much of the difference between the RRPA and the RRPAR cross sections is due to the inclusion of overlap integrals in the RRPAR calculations which lead to an approximately 19.4% reduction. It has been noted elsewhere [5,6] that the RRPA and RRPAR results for the total photoionization cross section tend to merge at photoelectron energies well above threshold.

With the normalization scheme used here, the experimental data [7] between the $4f$ thresholds and the $5p$ thresholds is considerably higher than the theoretical predictions. This is well below the region of autoionizing below the $5p$ thresholds. This is a discrepancy which deserves further study.

The photoelectron angular-distribution asymmetry parameters, β_{4f} , are shown in Fig. 2. The experimental

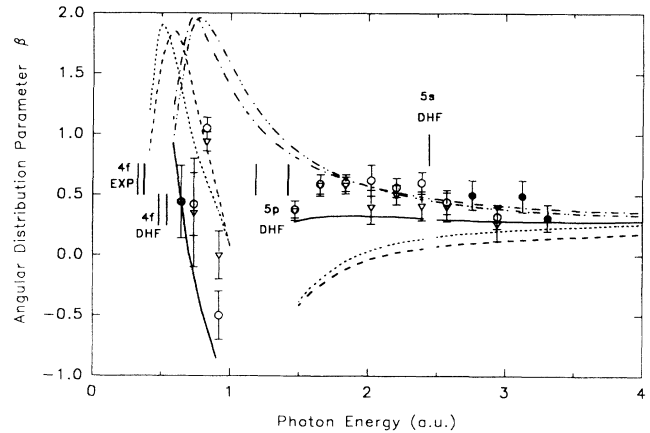


FIG. 2. Photoelectron angular-distribution asymmetry parameter β_{4f} for Yb. Solid curves are the RRPA length result. Long-dashed and short-dashed curves represent RRPAR length and velocity results, respectively. Dot-dashed and double-dot-dashed curves are truncated RRPA length and velocity results, respectively. Experimental data are from Ref. [7]; open circles are $4f_{7/2}$, open triangles are $4f_{5/2}$, and solid dots are both.

data are from Svensson *et al.* [7] and though the $4f_{7/2}$ and $4f_{5/2}$ angular-distribution parameters were reported separately, there is in fact very little difference between the two. The theoretical results are thus shown as the weighted average specified by Eq. (3). As may be seen, the β parameter is quite sensitive to various many-body effects in this case. To highlight this sensitivity, we show the results of a truncated eight-channel RRPA calculation including only the following relativistic dipole channels:

$$4f_{5/2} \rightarrow \epsilon g_{7/2}, \epsilon d_{3/2}, \epsilon d_{5/2}, \quad 4f_{7/2} \rightarrow \epsilon g_{7/2}, \epsilon g_{9/2}, \epsilon d_{5/2},$$

and

$$6s_{1/2} \rightarrow \epsilon p_{1/2}, \epsilon p_{3/2}.$$

This calculation is identical to that reported in the original paper by Svensson *et al.* [7] except that the weighted average of $4f_{7/2}$ and $4f_{5/2}$ has been taken here.

Comparison of the truncated RRPA calculation with the 15-channel RRPA result shows the strong effects of interchannel coupling between the $4f$ and $5p$ photoionization channels even below the $5p$ thresholds. The more complete RRPA calculation appears to assume the correct slope for the asymmetry parameter below 1 a.u. The inclusion of core relaxation in the RRPAR calculation introduces additional changes to the asymmetry parameter. The RRPAR calculation is in reasonable agreement with experiment below the $5p$ thresholds. However, just above the $5p$ thresholds, the RRPAR results are considerably lower than experiment [7].

Branching ratios $\sigma(4f_{7/2})/\sigma(4f_{5/2})$ were also calculated in the truncated RRPA, the RRPA, and the RRPAR and are presented along with the experimental measurements of Svensson *et al.* [7] in Fig. 3. The RRPA branching ratio begins well above the statistical ratio of $\frac{4}{3}$ because both the $4f_{7/2}$ and the $4f_{5/2}$ cross sec-

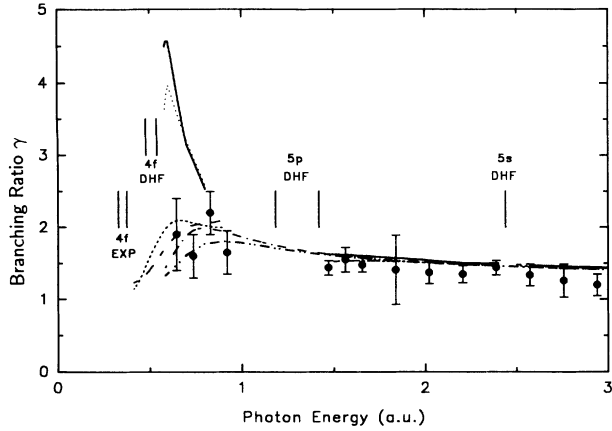


FIG. 3. Branching ratio $\gamma = \sigma(4f_{7/2})/\sigma(4f_{5/2})$ for atomic Yb. Solid curves and dotted curves represent length and velocity RRPA results, respectively. Long-dashed and short-dashed curves represent length and velocity RRPAR results, respectively. Dot-dashed curve and double-dot-dashed curve are truncated RRPA length and velocity results, respectively. Experimental data are ESSR measurements from Ref. [7].

tions are rising steeply above their thresholds in the RRPA calculations. Thus, the $4f_{7/2}$ partial cross section which begins at a lower threshold energy than the $4f_{5/2}$ partial cross section exceeds the $4f_{5/2}$ cross section by more than just the statistical value. The RRPAR calculation branching ratio begins below the $\frac{4}{3}$ statistical ratio because the cross sections are dropping toward a minimum just above the thresholds. Then when the cross sections begin to increase it is with a reduced slope compared with the RRPA. The agreement with experiment appears to be improved by the inclusion of relaxation effects.

B. The $4d$ subshell

Although the $4d$ subshell electrons are tightly bound to the Yb atom, the $4d$ subshell photoionization parameters are still strongly influenced by electron-correlation effects. Creating a vacancy in the $4d$ subshell changes the screening of all the outer electrons (including the large $4f$ subshell) thereby leading to substantial rearrangement effects. Also, the $4f$ cross section is still large well above the $4d$ threshold and is able to significantly influence the $4d$ photoionization channels.

The $4d$ photoionization cross sections calculated in various RRPA-type approximations are shown in Fig. 4. The RRPA calculation itself included nineteen jj -coupled photoionization channels, namely,

$$4d_{3/2} \rightarrow \epsilon f_{5/2}, \epsilon p_{1/2}, \epsilon p_{3/2}, \quad 4d_{5/2} \rightarrow \epsilon f_{5/2}, \epsilon f_{7/2}, \epsilon p_{3/2},$$

$$5s_{1/2} \rightarrow \epsilon p_{1/2}, \epsilon p_{3/2}, \quad 5p_{1/2} \rightarrow \epsilon d_{3/2}, \epsilon s_{1/2},$$

$$5p_{3/2} \rightarrow \epsilon d_{3/2}, \epsilon d_{5/2}, \epsilon s_{1/2}, \quad 4f_{5/2} \rightarrow \epsilon g_{7/2}, \epsilon d_{3/2}, \epsilon d_{5/2},$$

and

$$4f_{7/2} \rightarrow \epsilon g_{7/2}, \epsilon g_{9/2}, \epsilon d_{7/2}.$$

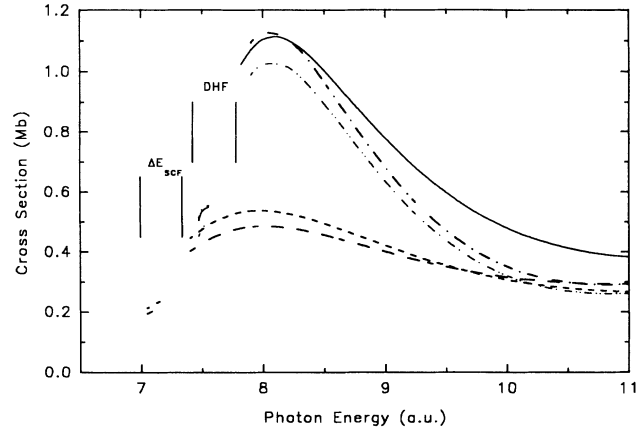


FIG. 4. Partial photoionization cross sections for the $4d$ subshell of Yb. Solid curves represent RRPA; long-dashed and short-dashed curves represent RRPAR length and velocity calculations, respectively; dot-dashed and double-dot-dashed curves represent length and velocity truncated RRPA, respectively.

Channels resulting from excitations of $4p$ and $4s$ electrons were excluded because of the large removal energies of these electrons. The truncated RRPA calculation included only $4d$ intrashell coupling among the channels

$$4d_{3/2} \rightarrow \epsilon f_{5/2}, \epsilon p_{1/2}, \epsilon p_{3/2}$$

and

$$4d_{5/2} \rightarrow \epsilon f_{5/2}, \epsilon f_{7/2}, \epsilon p_{3/2}.$$

The RRPAR calculation included the same nineteen channels as the RRPA calculation, but included relaxation effects as well. Thresholds used in the RRPAR calculation were the ΔE_{SCF} energies which are expected to contain most of the energy correlation for these deep inner shells.

Although the $4d$ cross section shown in Fig. 4 has a similar shape to the so-called giant resonances of the $4d$ cross sections of xenon, barium, and the lanthanides [1], it is much smaller in magnitude. This is presumably because of the large “effective Z ” in the potential of the $4d$ electrons. By comparing the RRPA result with the truncated RRPA result, it is possible to determine the influence of the $4f$ channels on the $4d$ cross section. The large $4f$ cross section (approximately 5.2 Mb at 10 a.u.) increases the magnitude of the $4d$ cross section at energies starting approximately 1 a.u. above the threshold.

The effects of relaxation are to be seen in the RRPAR cross section which has a peak value approximately 40% of the RRPA calculation, not including relaxation effects. Overlap integrals of the RRPAR method lead to approximately a 20% reduction in the partial $4d$ cross section. The remaining differences between the RRPA and the RRPAR cross sections are due to changes in the photoelectron potential from rearrangement of electrons external to the $4d$ subshell.

Photoelectron angular-distribution asymmetry parameters for $4d$ photoionization of Yb are shown in Fig. 5. In

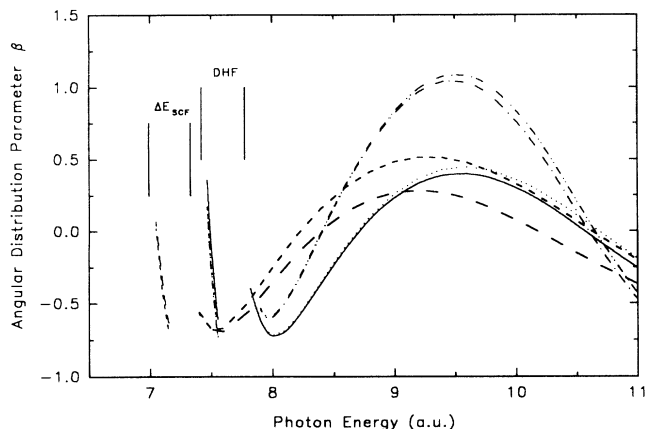


FIG. 5. Photoelectron angular-distribution asymmetry parameters β_{4d} for the $4d$ subshell of Yb. Solid and dotted curves represent RRPA length and velocity results, respectively. Long-dashed and short-dashed curves represent RRPAL length and velocity, respectively. Dot-dashed and double-dot-dashed curves represent truncated RRPA length and velocity, respectively.

this case, the effects of interchannel coupling are seen to be more significant than relaxation. The effect of the $4f$ channels on the $4d$ photoionization channels is to reduce the β parameter at its peak near 9 a.u., as may be noted by comparing the truncated RRPA result with the nineteen-channel RRPA result.

The branching ratios $\sigma(4d_{5/2})/\sigma(4d_{3/2})$ are shown in Fig. 6. Taking the differences in threshold energies into account, it is seen that the inclusion of relaxation effects has generally raised the branching ratio closer to the statistical ratio of $\frac{3}{2}$.

C. The $6s$ subshell

It is well known that the RRPA technique does not accurately describe photoionization from valence ns^2 sub-

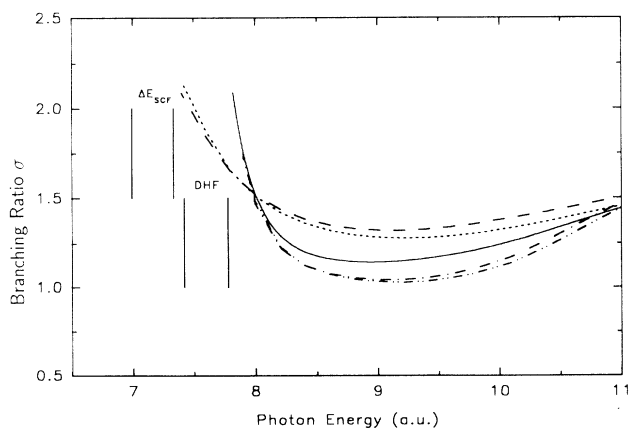


FIG. 6. Branching ratios $\gamma = \sigma(4d_{5/2})/\sigma(4d_{3/2})$ for Yb. Solid curve represents RRPA; long-dashed and short-dashed curves represent RRPAL length and velocity calculations, respectively; dot-dashed and double-dot-dashed curves represent truncated RRPA length and velocity results, respectively.

shells because of the double-electron resonances which occur just above the thresholds [12]. However, in regions where interchannel coupling is very important it is possible for the character of the ns^2 cross section and angular-distribution asymmetry parameter to be determined largely by correlations. In this study, RRPA-type calculations were carried out with and without interchannel coupling to determine the importance of correlation on the $6s$ photoionization cross section and angular-distribution asymmetry parameter. The fully coupled RRPA calculations included all 15 channels included in the calculation of the $4f$ cross sections whereas the truncated RRPA calculations included only two channels,

$$6s_{1/2} \rightarrow \epsilon p_{1/2}, \epsilon p_{3/2}.$$

Figure 7 shows the $6s$ cross sections with and without coupling with the $4f$ and $5p$ channels along with the experimental data [7] in this region. The experimental data were normalized so that the $4f$ cross section had the value 3.25 Mb at 40 eV as in the previous figures of this paper and as in Ref. [7]. The importance of interchannel coupling is seen clearly increasing the $6s$ cross section by an order of magnitude in places and changing the sign of the slope near the $4f$ threshold.

The Yb $6s$ angular-distribution asymmetry parameters are plotted in Fig. 8. As was noted for the cross sections, the effects of interchannel coupling are large. The dips in the truncated RRPA $6s$ β parameter arise when the dipole matrix elements for the two channels go through zeros at slightly different energies. Interchannel coupling, however, eliminates the Cooper minima that are present in the truncated RRPA calculations thus maintaining the β parameter closer to the value 2 predicted by theories neglecting the spin-orbit interaction.

IV. CONCLUSION

Both core-relaxation and interchannel-coupling effects have been found to be of importance in cross-section,

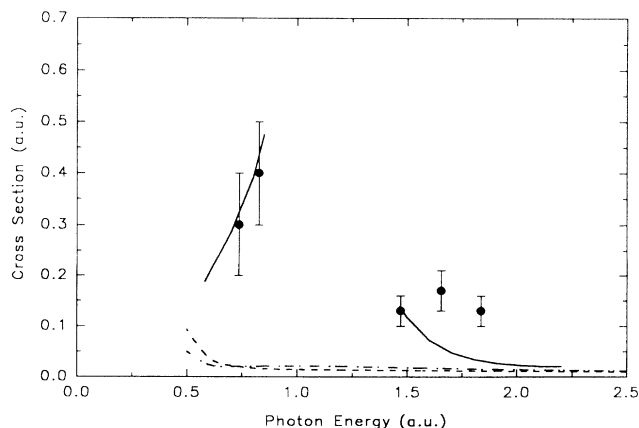


FIG. 7. Photoionization cross sections for the $6s$ subshell of Yb. Solid line is RRPA length calculation. Dashed and dot-dashed lines represent truncated RRPA length and velocity results, respectively. Experimental data are from Ref. [7].

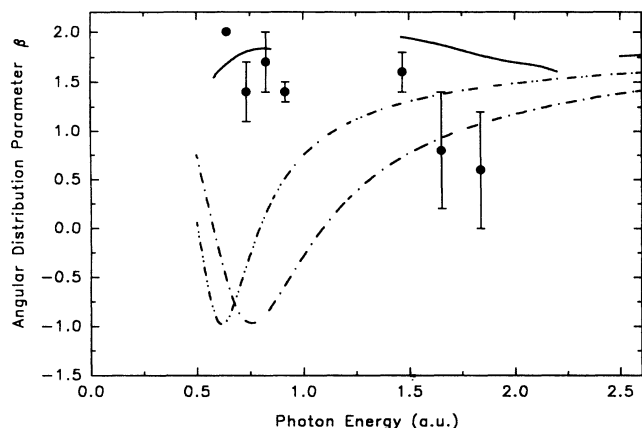


FIG. 8. Photoelectron angular-distribution asymmetry parameter β_{6s} for the $6s$ subshell of Yb. Solid lines represent RRPA length results. Dot-dashed and double-dashed lines represent truncated RRP length and velocity results, respectively. Experimental data are from Ref. [7].

branching-ratio, and angular-distribution asymmetry parameter calculations for $4f$ and $4d$ inner-shell photoionization of atomic ytterbium. As was noted in the case of atomic mercury [6], the inclusion of relaxation effects in RRPA-type calculations of $4f$ subshell cross sections tends to make an already flat distribution of oscillator strength even flatter. The RRPAR cross-section calculations are consistent with the renormalized measured cross sections [7] except between the $4f$ threshold and approximately 1 a.u., where the experimental data is con-

siderably larger than either the RRPA or the RRPAR. The effects of relaxation on the branching ratio $\sigma(4f_{7/2})/\sigma(4f_{5/2})$ and angular-distribution asymmetry parameter β_{4f} are also large. The inclusion of relaxation in calculations appears to improve agreement with the experimental branching ratio [7] near threshold, but does not give a good description of the angular-distribution asymmetry parameter β_{4f} above the $5p$ thresholds. The RRPA and RRPAR results tend to converge at higher photoelectron energies, demonstrating that high-speed photoelectrons are somewhat insensitive to the details of the potential.

The relatively small $4d$ partial cross section is profoundly affected by core relaxation due to the rearrangement of large outer subshells such as the $4f$ subshell. It is interesting that photoionization from a deep inner shell shows such strong many-body effects. It is hoped that this report will stimulate experimental work on this system.

Finally, it has been shown that the inclusion of interchannel coupling using the RRPA technique leads to reasonable agreement between theory and experiment [7] for the $6s$ partial photoionization cross and angular-distribution asymmetry parameter β_{6s} above the $4f$ thresholds.

ACKNOWLEDGMENTS

We wish to thank Walter Johnson for the use of the RRPA computer code. We thank Charles Tidwell for helpful discussions. This work was supported by NSF Grant No. PHY-9014012.

-
- [1] See, for example, *Giant Resonances in Atoms, Molecules, and Solids*, Vol. 151 of *NATO Advanced Study Institute, Series B: Physics*, edited by J. P. Connerade, J. M. Esteve, and R. C. Karnatak (Plenum, New York, 1987).
 - [2] M. Ya. Amusia, in *Atomic Photoeffect*, edited by P. G. Burke and H. Kleinpoppen, translated by K. T. Taylor (Plenum, New York, 1990), pp. 187–221.
 - [3] W. R. Johnson and C. D. Lin, *Phys. Rev. A* **20**, 964 (1979); W. R. Johnson, C. D. Lin, K. T. Cheng, and C. M. Lee, *Phys. Scr.* **21**, 403 (1980).
 - [4] V. Radojević, M. Kutzner, and H. P. Kelly, *Phys. Rev. A* **40**, 727 (1989).
 - [5] M. Kutzner, D. Winn, and S. Mattingly, *Phys. Rev. A* **48**, 404 (1993).
 - [6] M. Kutzner, C. Tidwell, S. Vance, and V. Radojević, *Phys. Rev. A* **49**, 300 (1994).
 - [7] W. A. Svensson, M. O. Krause, T. A. Carlson, V. Radojević, and W. R. Johnson, *Phys. Rev. A* **33**, 1024 (1986); M. Müller, N. Böwering, U. Heinzmann, V. Radojević, and W. Wijesundera, *J. Phys. B* **21**, L179 (1989).
 - [8] P. C. Deshmukh and S. T. Manson, *Phys. Rev. A* **34**, 4757 (1986).
 - [9] T. Åberg, in *Photoionization and Other Probes of Many-Electron Interactions*, edited by F. Wuilleumier (Plenum, New York, 1976), pp. 49–59.
 - [10] H. Siegbahn and L. Karlsson, in *Corpuscles and Radiation in Matter I*, edited by W. Mehlhorn, *Handbuch der Physik* Vol. 31 (Springer-Verlag, Berlin, 1982), p. 215.
 - [11] I. P. Grant, B. J. McKenzie, P. H. Norrington, D. F. Mayers, and N. C. Pyper, *Comput. Phys. Commun.* **21**, 207 (1980).
 - [12] M. Ya. Amusia, in *Atomic Photoeffect*, translated by K. T. Taylor (Plenum, New York, 1990), pp. 156–161.